Janusz Badur and Mateusz Bryk*

Analysis of unsteady boiling during high-temperatured body dipping in water

Energy Conversion Department, Institute of Fluid Flow Machinery, Polish Academy of Sciences, 80-231 Gdansk, Fiszera 14, Poland

Abstract

In this paper, the analysis of sudden water phase change during high-temperature metal body dipping is presented. According to that purpose, the computational fluid dynamic analysis has been carried out. The nonstationarity and behavior of sudden water phase change has been examined. The calculation model consists of the solid domain (vessel and high-temperature metal) and fluid domain (liquid filling vessel). The metal body insertion to the fluid domain was obtained by the use of dynamic mesh. Special case of the dipping velocity, the metal body of temperature 723 K and fluid temperature 288 K. was examined. Moving on to calculations, the model containing basic conservation equation, expanded of turbulence and liquid evaporation equations has been used.

Nomenclature

A	–	interfacial area density, 1/m
E	–	heat sources due to mass transfer and wall heat transfer
e_b	–	blackbody irradiance, radiative heat flux, W/m^2
e	–	total energy, J
g	–	specific radiative energy, J/m^{2}s
I	–	specific internal energy, J/kg
i'	–	boundary value of radiative intensity, W/m^{2}sr
K	–	drag function

*Corresponding Author. Email adress: mbryk@imp.gda.pl

M – molar mass, kg/kmol
$\dot{m}$ – rate of mass transfer, kg/m^{3}s
N – bubble number density, kg/m^3
P – pressure, N/m^2
P_{sat} – pressure in saturation dome, Pa
R – exchange function describing heat transfer between fields
R – gas constant, kJ/kmol K
T – temperature, K
t – time, s
$\mathbf{v}$ – velocity
$\mathbf{x}$ – position vector
S_k – k source, kg/m^{3}s
S_ε – sources, kg/m^{4}s

Greek symbols

α – vapor volume fraction, absorption coefficient, 1/m
β – accommodation coefficient
θ – void fraction
λ – heat conduction, W/mK
ρ – density, kg/m^3

Subscripts and superscripts

b – bubble
d – droplet or liquid phase
i – interfacial
s – steel
sat – saturation
v – vapor

Keywords: CFD modeling; Numerical analysis

1 Introduction

The commonly known thermal treatment of materials type is hardening. In short, hardening is based on material heating to high temperature in order to obtain austenite phase, then endurance in this temperature, and finally fast cooling in order to obtain martensite or bainite phase. The cooling mentioned above takes place through the hardening bath. In this bath water, mineral oil, emulsions and other fluids are in use.

Our attention focused on water and phenomenon which occurs during dipping the high temperature body in water. During the contact of hot metal body with water's surface, the phase change occur, evaporation and then boiling near the

surface of submerged metal body. It can be even said that water simply cracks as a result of the sudden large temperature change. The similar analogy was analyzed in [3], where to the cool glass material, the hot fluid is poured.

In this study, the modeling of the flow with evaporation and boiling of water where three phase flow occurs, was tried to be solved. Additionally, the dynamic mesh was used in order to simulate the metal body motion. Phenomenon which occur during hardening are commonly known, however the three phase flow, which occurs here, has not been numerically modeled so far, this is the reason of our investigation. There is a lot of works about quenching, for example [7,10,12], but authors are focused on the steel domain, not on the fluid domain. One example of vapor blanket during quenching by submerging is shown in [13]. Authors of this work could not find articles about numerical simulations about fluid behavior during quenching.

In the simulation, the three phase flow occurs because we have to deal with water, vapor, and air domain. In terms of multiphase flows, a lot of information can be found in literature [1–6,8,11,14,15]. From mentioned earlier works, the authors obtained data and information about phenomenon which occur during evaporation and boiling process.

2   Analyzed system

The rectangular steel body which is submerged to the volume of water with constant velocity is set as analyzed system. The whole system is shown in Fig. 1. The main dimensions of analyzed system, shown in Fig. 2., are: 214 mm×110 mm for the tank and 25 mm×50 mm for the steel body.

The discretization of the model was obtained by two type of the mesh elements, by square and triangular ones. In Fig. 3a we can see the mesh with a number of elements about 500 000. This solution was applied because of the dynamic mesh use necessity. In solution, the shape of the domain is changing with time due to motion on the domain boundaries. The dynamic mesh mode is applied to multiphase flow. The model provides the motion implemented via user defined function (UDF). In this study, the motion is specified on a face zone (i.e. steel domain). The principle of operation of this solution consists on triangular mesh deformation by square mesh. As is shown in Fig. 3a, the metal body is discretized by square elements, exactly this mesh will deform triangular elements which are shown in Fig. 3b. During the movement of the solid the triangular elements are smoothing and remeshing occurs. The precise description and the principle of operation can be found in [9].
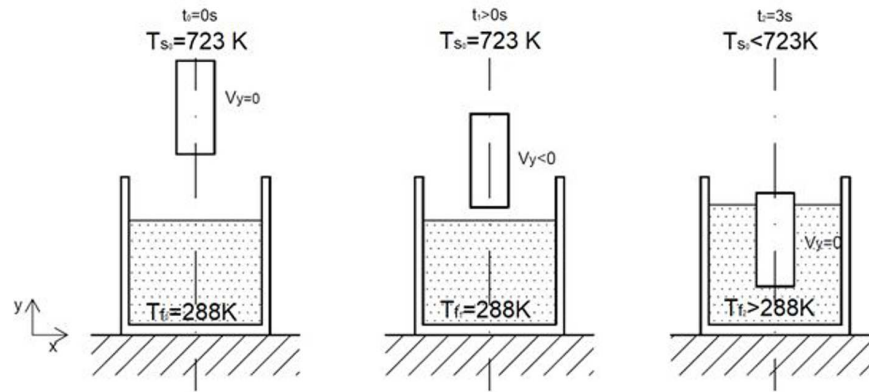
Figure 1: Cross section of analyzed system at three time steps $t_0 = 0$ s, $t_1 > 0$ s, and $t_1 = 3$ s, T_{S_0}, T_{f_0}, T_{f_1}, and T_{f_2} – temperature of steel body and fluid, respectively, v_y – velocity of steel body.
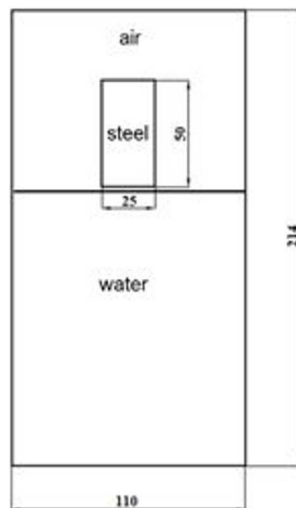

Figure 2: Main dimensions of analyzed system in millimeters.

3 The set of equations

For the fluid flow simulation, three basic formulas of conservation are fulfilled. These three main formulation which describe computational fluid dynamics (CFD) are presented below [3–5]:
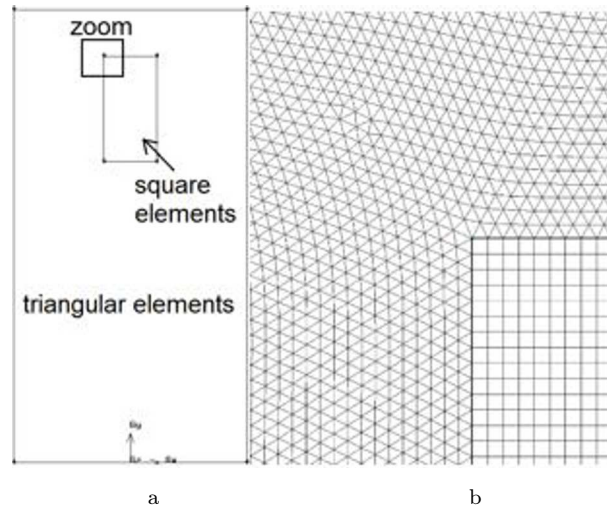
Figure 3: Discretization of analyzed system.

conservation of mass equation:

$$\partial_t (\rho) + \mathrm{div}\,(\mathrm{P}\,\overrightarrow{v}) = 0 \;, \tag{1}$$

conservation of momentum equation:

$$\partial_t (\rho\overrightarrow{v}) + \mathrm{div}\,(\rho\overrightarrow{v} \otimes \overrightarrow{v} + \mathrm{PI}) = \mathrm{div}\,\overrightarrow{\tau}^{\,\mathrm{c}} + \rho\,\mathrm{b} \;, \tag{2}$$

conservation of energy equation:

$$\partial_t (\rho e) + \mathrm{div}\left[\left(\mathrm{e} + \frac{\mathrm{P}}{\rho}\right)\rho\,\overrightarrow{v}\right] = \mathrm{div}\left(\overrightarrow{q} + \overrightarrow{q}^{\,\mathbf{t}} + \overset{\leftrightarrow\mathrm{c}}{\tau}\overrightarrow{v} + \overrightarrow{q}^{\,\mathrm{D}} + \overrightarrow{q}^{\,\mathrm{rad}}\right) + \rho\,\overrightarrow{b}\,\overrightarrow{v} \;. \tag{3}$$

These are balance equations in conservative form, where: ρ – gas density, $\overset{\leftrightarrow c}{\tau} = \overrightarrow{t} + \overrightarrow{R} + \overrightarrow{D}$ – total tensor of irreversible stress, $\overrightarrow{v} = v_i \overrightarrow{e}_i$ – mean velocity, $\overrightarrow{q}$ – molecular heat flux, $\overrightarrow{q}^{\,\mathbf{t}}$ – turbulent heat flux, $\overrightarrow{q}^{D}$ – diffusive heat flux, $\overrightarrow{q}^{rad}$ – radiation heat flux, P – pressure, $e = u + \frac{1}{2}\,\overrightarrow{v} \cdot \overrightarrow{v}$ – total energy, $\overrightarrow{b} = -9.81\,\overrightarrow{e}_z$, here $\overrightarrow{e}_z$ denotes unit vector in axial direction, $\mathbf{I}$ is the identity tensor and $\otimes$ is the outer product (the Kronecker product).

The above three equation are complemented by two evolution equations for parameters, which allow to define tensile tensor components [4]:

evolution equation concerning turbulent energy k:

$$\partial_t (\rho k) + \mathrm{div}\,(\rho\mathrm{k}\,\overrightarrow{v}) = \mathrm{div}(\overrightarrow{J}_{\mathrm{k}}) + \mathrm{S}_{\mathrm{k}} \;, \tag{4}$$

evolution equation concerning energy dissipation ε:

$$\partial_t \left(\rho\varepsilon\right) + \mathrm{div}\left(\rho\varepsilon\,\overrightarrow{v}\right) = \mathrm{div}(\overrightarrow{J}_\varepsilon) + \mathrm{S}_\varepsilon \ . \tag{5}$$

A more detailed description of the used models in CFD codes can be also find in [2,4]. The pressure of the liquid walls is omitted as the pressure which causes negligible stresses in walls. Because of that, the equation of momentum conservation is not important due to the mechanical reasons but only due to thermal reasons, as the equation which describes heat convection and movement of the fluid, which is heating by contact with the hot wall. For that reason, the viscous and turbulent stresses influence is negligible. More important is the assumption of gravity in element of mass force, $\rho\left(\overrightarrow{x}, t\right)\overrightarrow{b}$, or a precise equation of water state which gives actual water density in each point and in each moment, $\rho(\mathbf{x}, t)$.

4 Phase change model

The pressure-based phase change model applied in this study uses coefficients for boiling delay behaviors accounted for thermal non-equilibrium. The transport equation for the phase change is given by [8,14,15]:

$$\partial_t \left(\alpha_v \rho_v\right) + \nabla \cdot \left(\alpha_v \rho_v \overrightarrow{v}_{\mathrm{m}}\right) = \dot{m} \ . \tag{6}$$

The source term $\dot{m}$ is defined as follows [14,15]:

$$\dot{m} = A_i \beta \sqrt{\frac{M}{2\pi \mathrm{R} T_{sat}}} (P_v - P_{sat}) \ , \tag{7}$$

where $P_v = P_{sat} + 0.195\rho k$ depends on the turbulent kinetic energy and the interfacial area density A_i is given by formula

$$A_i = (6\alpha_v)^{\frac{2}{3}}(\pi N)^{1/3} \ , \tag{8}$$

where N is the bubble number density.

Additionally, the model has been expanded by Lee model [11]. In this model, separate conservation equations are formulated for each phase and the interaction between the phases is taken into account for by including evaporation, interfacial drag, and interfacial heat transfer terms in the corresponding mass, momentum, and energy equations. The model assumes that the effects of drag-dissipation and pressure compression energy associated with the void fraction and volume change

are distributed to both phases.

In Lee model the energy conservation is given by formula

$$\rho'_d \left[\partial_t (I_d) + \nabla \cdot \left(\overrightarrow{U}_d I_d \right) - I_d \nabla \cdot \overrightarrow{U}_d \right] = E_d + R(T_v - T_d) +$$
$$\theta_d K \left(\overrightarrow{U}_d - \overrightarrow{U}_v \right)^2 + \nabla k_d \theta_d \nabla T_d + V_{id} - P \theta_d \nabla \overrightarrow{U}_d \qquad (9)$$

for the liquid phase and

$$\rho'_v \left[\partial_t (I_v) + \nabla \cdot \left(\overrightarrow{U}_v I_v \right) - I_v \nabla \cdot \overrightarrow{U}_v \right] = E_v + R(T_d - T_v) +$$
$$\theta_v K \left(\overrightarrow{U}_d - \overrightarrow{U}_v \right)^2 + \nabla k_v \theta_v \nabla T_v + V_{iv} - P \theta_v \nabla \overrightarrow{U}_v \qquad (10)$$

for the vapor phase, where the prime symbol, ρ', denotes specific density, I is the specifc internal energy . The volume fractions of liquid and vapor phases satisfy the condition

$$\theta_d + \theta_v = 1 . \qquad (11)$$

5 Radiation model

Because of high value of steel temperature, radiation model [2,16] has been included in numerical code. The radiation influence is visible in transport of momentum. The additional transport of momentum is defined by radiative energy flux as follows:

$$\overset{\leftrightarrow}{\tau}^{rad} = \left(\delta_{ij} \frac{\varphi_1}{3} + \varphi_2 \Lambda_i \Lambda_j \right) \overrightarrow{e}_i \otimes \overrightarrow{e}_j , \qquad (12)$$

where

$$\varphi_1 = -1 + \sqrt{4 - 3\lambda} ,$$

$$\varphi_2 = \frac{2 - \sqrt{4 - 3\lambda}}{\lambda} ,$$

$$\Lambda_i = \frac{q_i^{rad}}{\sqrt{\lambda}},$$

$$\lambda = \overrightarrow{q}^{rad} \cdot \overrightarrow{q}^{rad}$$

and $\overrightarrow{q}^{rad}$ is defined as

$$\nabla \cdot \overrightarrow{q}^{rad} = \alpha \left[4e_b - g \right] , \qquad (13)$$

where: δ_{ij} – the Kronecker delta, i,j – main directions, α absorption coefficient, e_b – blackbody irradiance, radiative heat flux, g – specific radiative energy. The radiative energy is defined by formula

$$g = \int_{4\pi} i' d\hat{\omega}'$$

in which, i' describes the boundary value of radiative intensity and $\hat{\omega}'$ is solid angle.

6　Boundary and initial condition

The following boundary conditions have been assumed:
   – water liquid temperature 288 K,
   – steel body temperature 723 K,
   – air temperature 288 K ,
   – steel body velocity $v_y = \begin{cases} -0.06 \ \frac{\text{m}}{\text{s}} & \text{if} \quad t \leq 1 \ \text{s} \ , \\ \ \ 0.00 \ \frac{\text{m}}{\text{s}} & \text{if} \quad t > 1 \ \text{s} \ . \end{cases}$

In Fig. 4, the individual surfaces and domains are presented. There is no inlet surface, because of injection of steel body to the water domain. The coordinate system is the reason why the velocity value is negative. The velocity value is negative because of Oy-axis direction.
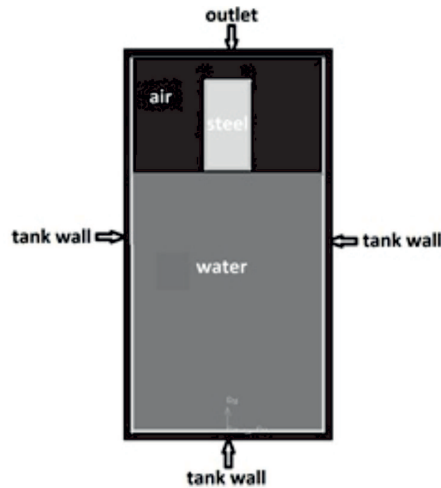

Figure 4: Designation of analyzed system.

At the beginning of the simulation, 0.0005 s time step has been set. The low value of time step results from the phenomena rapidity. Then after 1 s, when the steel body movement is stopped, time step increases to 0.005 s. The whole simulation runs in time of 3 s. As it can be seen in Fig. 5, after the initialization process, only water, air and steel domain occur. The initial volume of vapor is set to 0.
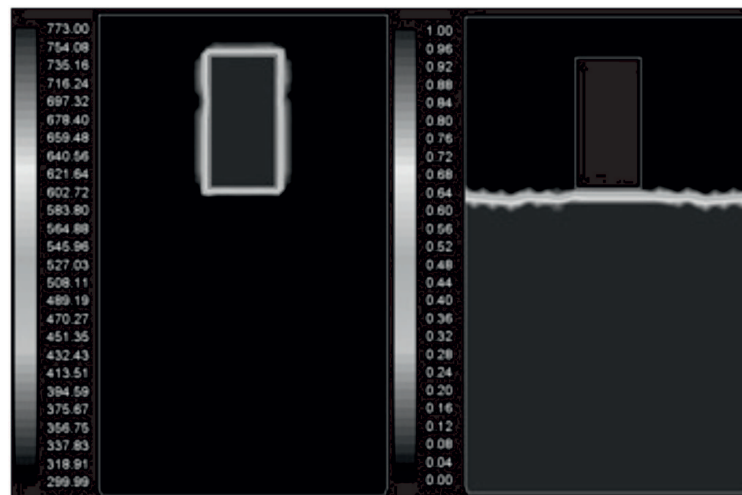

Figure 5: Temperature and volume of water at the beginning the simulation.

7 Numerical results

In Figs. 6–7 numerical results of simulation are presented. The generated steam and the water behavior is shown at the same time. In order to catch sight of the differences during the simulation, 19 photos in 19 different moments for water and vapor domain are shown. It was impossible to show both water and vapor behaviors in one picture, that is the reason the vapor and water are shown separately. Additionally, in the pictures the time steps values, when discussed phenomenon occur are presented.

In Fig. 6 it can be observed vapor volume fraction and in Fig. 7 water volume fraction. It can be seen that at the beginning of the simulation in time 0.0025 s, the volume of steam under the bottom wall of steel body is developing. The reason of mentioned above phenomenon occurrence is temperature distribution thanks to radiation from steel body to the water surface which starts to evaporate because

of sudden temperature change. The implemented model shows the process of the formation and the behavior of the vapor.

It is also clear to see that the vapor, right after the steel body dipping in water, forms from the steel body top surface. There is no visible the sudden-creation of the vapor bubbles near the water-dipping edges as a result of boiling. As has been mentioned above, the saturated vapor form has the source on the steel body top surface. The reason of this phenomenon is the wet steam transport (vapor quality <1), which forms by water evaporation from the surface air-water and its hoarding on the upper steel body surface, which has higher temperature than the rest of steel domain dipped in the water. The wet steam, which abuts with the high-temperature upper steel body surface, underlines sudden heating up to saturation state. After that, as a result of lower density than the water, the vapor float up [14,15]. This process occurs cyclically over time. At one moment, the water domain thank to heating by steel body has higher temperature and that is why the dry vapor creation process progress faster and last less time.
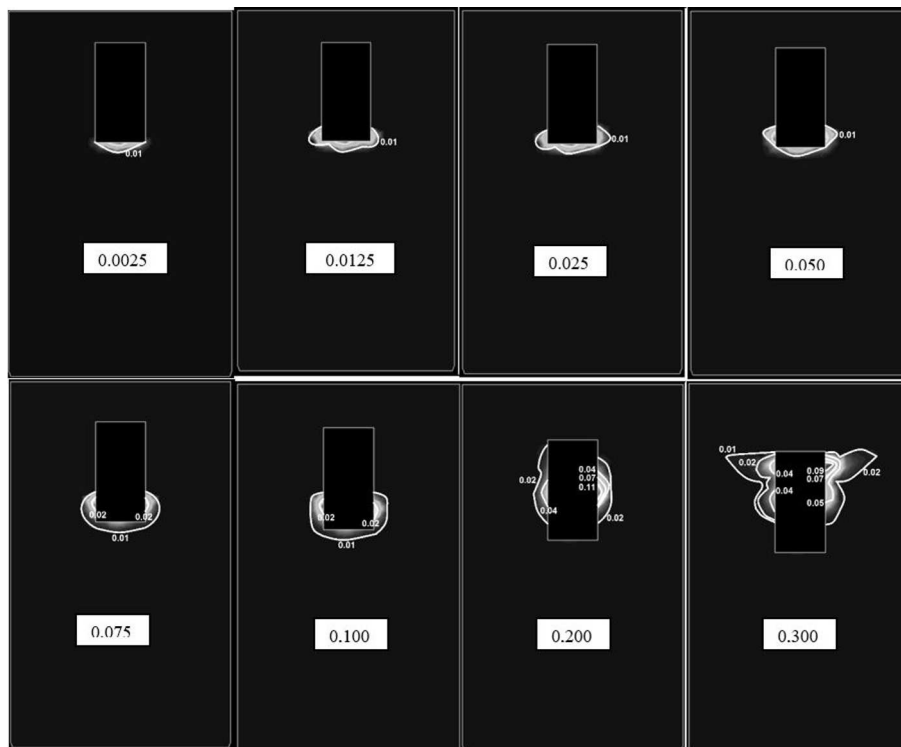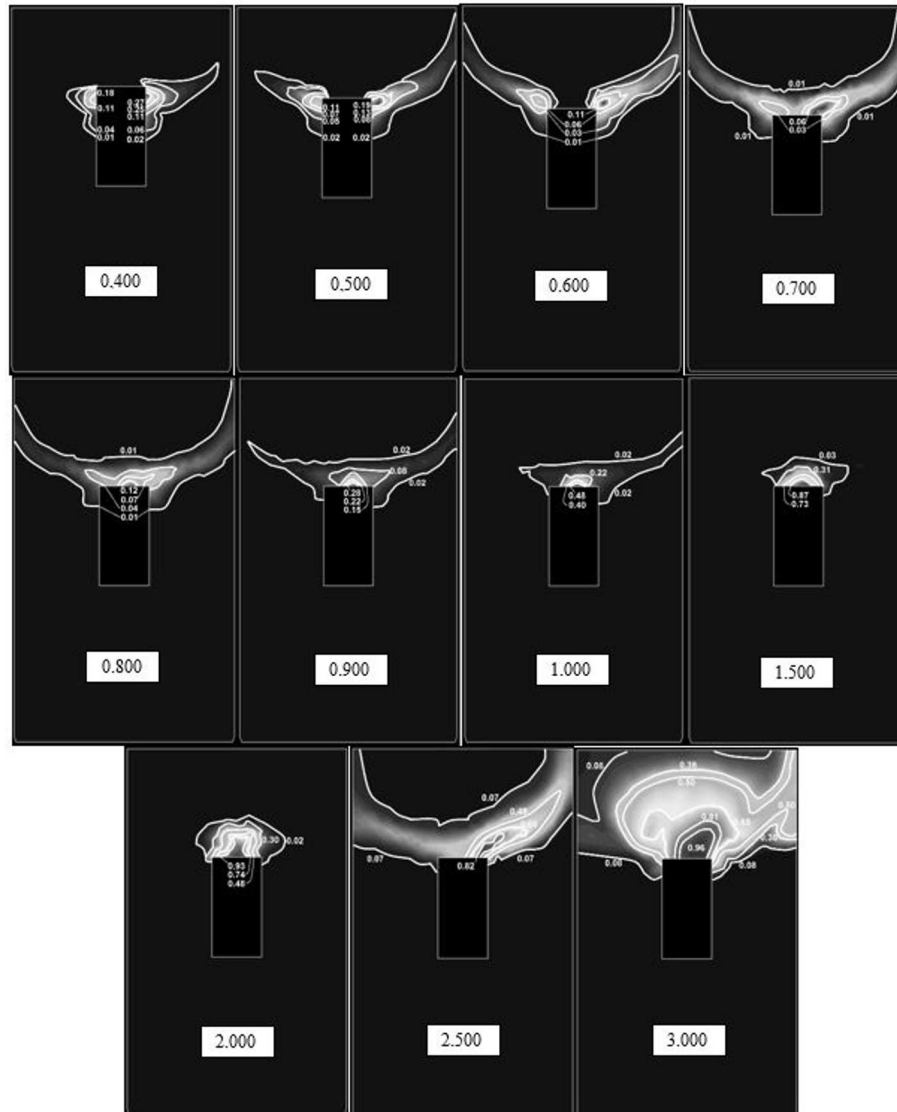

to Fig.6

Figure 6: Vapor forming and behavior in examined phenomenon.

Going to the water behavior, it can be observed that whole water level is subjected directly the state change. However it is not change from water to dry vapor, we can see that as a result the steel body injection, which is at high temperature, the wet steam layers forms. This phenomenon is visible especially in the phase boundary air-water. Also the wet steam forms on the wet-dipped

steel body surfaces, it is clear to see in the part 0.1–1.0 s of the simulation. In the enclosed figures it can be seen that wet steam redistribution in analyzed system (air domain) occurs (part 2–3 s of the simulation).
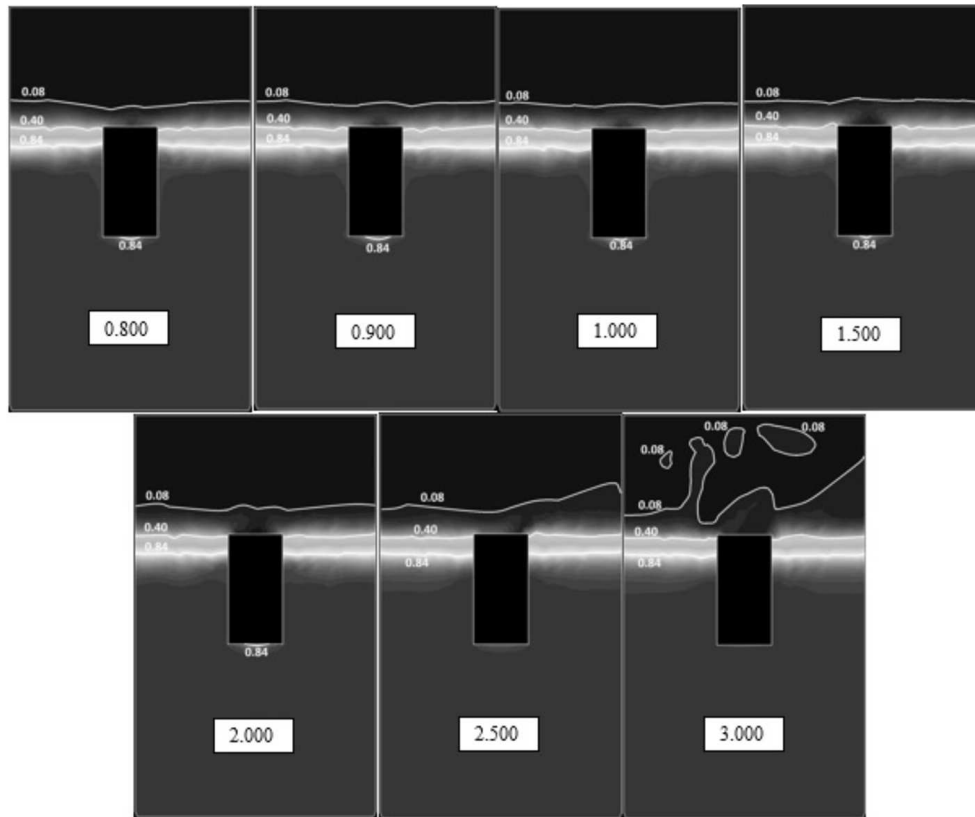

to Fig. 7

Figure 7: Time-dependent behavior of water in examined phenomenon.

8   Conclusions

The numerical code implementation and carried out simulation mapped with good accuracy the water behavior during the high-temperature steel body dipping. As it can be seen, we could not simulate the vapor bubbles creation which occurs during the boiling process. During the quenching process only evaporation process on the water surface can be seen. Additionally, no bubbles are formed during the quenching. Because of that, we can say, that the evaporation process in terms of physics is acceptable. We need to mention that not always the vapor bubbles form. The boiling process depends on a lot of the conditions, such as the dipping-body surface roughness, which determines the vapor bubbles form ability [13–15].

Received in May 2017

References

[1] Ahmed Wael H., Ching Chan Y., Shoukri M.: *Local void fraction and liquid turbulence measurements of two-phase flow downstream of a sudden expansion.* Trans. Inst. Fluid-Flow Mach. **118**(2006), 3–74.

[2] Badur J.: *Numerical modeling of well-balanced combustion in gas turbines.* IMP PAN Gdańsk, 2003 (in Polish).

[3] Badur J., Bryk M., Ziółkowski P., Sławiński D., Ziółkowski P., Kornet S., Stajnke M.: *On a comparison of Huber-Mises-Hencky with Burzyński-Pęcherski equivalent stresses for glass body during nonstationary thermal load.* In: AIP Conf. Proc. **1822**(2017), 020002.

[4] Badur J.: *Five lectures of contemporary fluid termomechanics.* Gdańsk 2005 (in Polish).

[5] Badur J.: *The Energy notion evolution.* Wydawnictwo IMP PAN Gdańsk, 2009 (in Polish).

[6] Bilicki Z., Kwidziński R.: *Viscous term in the model of two-phase bubble flow.* Trans. Inst. Fluid-Flow Mach. **99**(1995), 79–88.

[7] Bineli A.R.R., Jardini L. A., Filho M.R.: *Investigation of heat transfer coefficient using CFD simulation in quenching process.* 20th Int. Cong. of Mechanical Engineering, Gramado, Nov. 15-20, 2009.

[8] Dang Le, Quang & Besagni, Giorgio & Inzoli, Fabio & Mereu, Riccardo.: *Numerical Investigation of Flash Boiling Flow Inside Nozzle: Sensitivity Analysis on Turbulence Modeling Approaches.* In: Proc. CHT-17 ICHMT Int. Symp. on Advances in Computational Heat Transfer, Napoli, May 28 – June 1, 2017.

[9] *Dynamic Mesh Theory.* Release 16.2 Fluent, 2016.

[10] Gur H., Simsir C.: *Simulation of quenching: A Review.* Mater. Perform. Charact. **1**(2012), 1 104479. 10.1520/MPC104479, .

[11] Lee W.H.: *A pressure iteration scheme for two-phase flow modeling.* Techn. Rep. LA-UR 79-975. Los Alamos Scientific Laboratory, Los Alamos, 1979.

[12] Barrena-Rodriguez M., *et al.*: *An efficient fluid-dynamic analysis to improve industrial quenching systems.* Metals **7**(2017), 190. DOI:10.3390/met7060190.

[13] Passarella N.D., Varas F., Martin B.E.: *Development of a heat transfer model for quenching by submerging.* Mecánica Computacional XXIX(2010), 57, 5773–5783.

[14] Rohsenow M. W., Hartnett J.P., Young I.C.: *Handbook of Heat Transfer.* MG-H, New York, 1998.

[15] Thome J.R.: *Engineering Data Book III.* Wolverine Tube, Inc, Lausanne 2006.

[16] Yufang Zhang.: *Coupled convective heat transfer and radiative energy transfer in turbulent boundary layers.* Other. Ecole Centrale Paris, 2013.